

Associated Absorption Lines in the Radio-Loud Quasar 3C 351: Far-Ultraviolet Echelle Spectroscopy from the Hubble Space Telescope

Q. YUAN^{1,2}, R. F. GREEN², M. BROTHERTON², T. M. TRIPP³, M. E. KAISER⁴, G. A. KRISS⁵

ABSTRACT

As one of the most luminous radio-loud quasars showing intrinsic ultraviolet (UV) and X-ray absorption, 3C 351 provides a laboratory for studying the kinematics and physical conditions of such ionized absorbers. We present an analysis of the intrinsic absorption lines in the high-resolution ($\sim 7 \text{ km s}^{-1}$) far-UV spectrum which was obtained from observations with the *Space Telescope Imaging Spectrograph* (STIS) on board the *Hubble Space Telescope* (HST). The spectrum spans wavelengths from 1150 Å to 1710 Å, and shows strong emission lines from O VI and Ly α . Associated absorption lines are present on the blue wings of the high-ionization emission doublets O VI $\lambda\lambda$ 1032,1038 and N V $\lambda\lambda$ 1238,1242, as well as the Lyman lines through Ly ϵ . These intrinsic absorption features are resolved into several distinct kinematic components, covering rest-frame velocities from -40 to -2800 km s^{-1} , with respect to the systemic redshift of $z_{em} = 0.3721$. For the majority of these absorption line regions, strong evidence of partial covering of both the background continuum source and the broad emission line region (BELR) is found, which supports the intrinsic absorption origin and rules out the possibility that the absorption arises in some associated cluster of galaxies. The relationship between the far-UV absorbers and X-ray ‘warm’ absorbers are studied with the assistance of photoionization models. Most of the UV associated absorption components have low values of the ionization parameter and total hydrogen column densities, which is inconsistent with previous claims that the UV and X-ray absorption arises in the same material. Analysis of these components supports a picture with a wide range of ionization parameters, temperatures, and column densities in AGN outflows.

¹Department of Physics, Nanjing Normal University, NingHai Road 122, Nanjing 210097, China; yuan@noao.edu; qirongwy@public1.ptt.js.cn

²Kitt Peak National Observatory, National Optical Astronomy Observatory, 950 N. Cherry Ave., P.O. Box 26732, Tucson, AZ 85726-6732; green,mbrother@noao.edu

³Princeton University Observatory, Princeton, NJ 08544

⁴Department of Physics and Astronomy, Johns Hopkins University, Baltimore, MD 21218

⁵Space Telescope Science Institute, 3700 San Martin Drive, Baltimore, MD 21218

Subject headings: quasars:absorption lines — quasars:individual (3C 351) — ultra-violet: galaxies — X-rays: galaxies

1. INTRODUCTION

It has been recently appreciated that the ionized (or so-called “warm”) gas that produces intrinsic absorption in the X-ray spectra of low-luminosity Active Galactic Nuclei (AGNs) (e.g., Seyfert 1 galaxies) is an important, newly recognized component of their near-nuclear structure. Recent X-ray spectroscopic observations indicate that more than half of Seyfert 1 galaxies show K-shell absorption edges of warm oxygen (O VII and O VIII) characteristic of photoionized gas (Reynolds 1997; George et al. 1998). Moreover, a similar fraction show intrinsic absorption associated with their active nuclei in their ultraviolet (UV) spectra, and there appears to be a one-to-one correspondence between objects showing X-ray and UV absorption, suggesting that these two phenomena are related (Crenshaw et al. 1999).

The amount and presence of intrinsic absorption are found to depend upon either the luminosity or radio properties of AGNs: the narrow “associated” ($z_{ab} \approx z_{em}$) UV and X-ray “warm” absorbers are rare in high-luminosity and radio-loud quasars (Nicastro et al. 1999). Among high-luminosity quasars, intrinsic broad absorption lines (BALs) spanning up to tens of thousands of km s^{-1} are seen in about 10-20% of quasars, with a decrease in outflow velocity in the radio-loud quasars (Becker et al. 2001). BAL quasars are also deficient in X-rays (Green et al. 2001; Gallagher et al. 2002). The luminous radio-loud quasars with narrow absorption lines (NALs) appear to bridge the Seyfert warm absorbers and the BAL quasars, and may possess different physical conditions. This category includes two well studied radio-loud quasars, namely, 3C 351 (Fiore et al. 1993), and 3C 212 (Mathur et al. 1994), which are found to have ionized absorbers. In the current paper we pursue more detailed investigations of the the associated UV absorbers in 3C 351 based on a high-resolution far-UV spectrum.

Observationally, the radio-loud quasar 3C 351 ($z_{em} = 0.3721$; Marziani et al. 1996) is very lobe-dominated with only 0.65% of the flux density from the compact core at 6 cm (Kellermann et al. 1989), showing two opposite jets of similar angular extent. This FR II source has a steep radio spectrum and a low ratio of radio core luminosity at 5 GHz to optical V-band continuum luminosity ($\log R_V \sim 0.73$; Brotherton 1996), indicating an edge-on geometry of the central engine. Additionally, 3C 351 is also rather X-ray-“quiet” with a factor of ~ 5 lower X-ray flux than the average radio-loud quasar (Wilkes et al. 1994). Its effective optical-to-X-ray slope α_{ox} is 1.55 (Tananbaum et al. 1986), as compared to $\alpha_{ox} = 1.3$ for an average radio-loud quasar. Even though 3C 351 is X-ray quiet, among radio-loud quasars known to have ionized absorption, it is one of the most X-ray luminous ($L_{0.1-2\text{keV}} = 2.3 \times 10^{45} \text{ ergs s}^{-1}$; Fiore et al. 1993), and therefore it is an excellent test case for studying the kinematics and physical conditions of the

absorbing outflow associated with the nucleus of a radio-loud quasar.

The *ROSAT* Position Sensitive Proportional Counter (PSPC) observations show that the dominant feature in its X-ray spectrum is a strong O VII and/or O VIII absorption edge. A factor of 1.7 change in flux was found between observations in 1991 October and 1993 August, which stimulated a test of ionization models for the warm absorber in 3C 351, under the simplest photoionization equilibrium (Nicastro et al. 1999). Moreover, as a part of the Quasar Absorption Lines Key project (Bahcall et al. 1993), an intermediate-resolution ($R \sim 1300$) UV spectrum of 3C 351 was taken with the Faint Object Spectrograph (FOS) of the *HST*. As a result, a strong absorption system at $z = 0.3646$ was found in the high-ionization doublets of O VI, N V, and C IV, as well as in the Lyman series from Ly α to Ly δ . It was suggested by the authors that these UV absorption lines are due to an associated cluster of galaxies. However, no compelling evidence of the cluster was found in follow-up studies (Ellingson et al. 1994; Lanzetta, Bowen, Tytler, & Webb 1995; Le Brun, Bergeron, & Boisse 1996). In this paper we provide profound evidence that this associated absorption system is an intrinsic absorber located close to the QSO nucleus.

To what extent do the UV and X-ray absorbers arise in the same regions? This is an important question for understanding the structure of quasar nuclei. In the case of 3C 351, Mathur et al. (1994) proposed a simple one-zone photoionization model and claimed that the UV absorption features are due to the same material detected in the X-ray observations. To answer this question, quasi-simultaneous high-resolution UV and X-ray spectra of intrinsic lines should be taken. We notice that the UV absorptions presented in previous studies are typically comprised of multiple kinematic components (Crenshaw et al. 1999; Kriss et al. 2000). High-resolution spectroscopic observations allow accurate determination of absorption width and resolve multiple components, which is the key in determining the column density and velocity structure along the line of sight.

The Space Telescope Imaging Spectrograph (STIS) was installed during the second servicing mission of *HST*, and the high-resolution *E140M* and *E230M* echelle modes of this instrument are ideally suited for the study of associated UV absorbers. In this paper we present a high-resolution, far-UV STIS spectrum of 3C 351 covering the O VI $\lambda\lambda 1032, 1038$, N V $\lambda\lambda 1238, 1242$ and the Lyman series (§2). We focus on resolving the kinematic components in the associated absorption (§3), and interpret the spectral features with the assistance of photoionization models (§4). Then, we discuss our findings together with previous results for a better understanding of the ionized outflow of 3C 351 (§5). Finally, a summary is given (§6).

2. OBSERVATIONS

High-resolution echelle spectra of 3C351 were obtained with STIS on four occasions between 1999 June 27 and 2000 July 25. A brief log of the observations is provided in Table 1

including the date, total exposure time, and *HST* archive identification codes for each observation. Individual exposure durations ranged from 2230 to 2500 seconds, and wavelength calibration exposures were obtained between the individual observations of the quasar. All of the observations employed the intermediate-resolution *E140M* echelle mode of STIS with the $0''.2 \times 0''.06$ slit; this mode provides a resolution of 7 km s^{-1} (FWHM) with nearly complete wavelength coverage from 1150 – 1710 Å (There are only four small gaps between orders at $\lambda > 1634 \text{ Å}$). A complete description of the design of STIS has been provided by Woodgate et al. (1998), and Kimble et al. (1998) assess the on-orbit performance of the instrument.

The data were reduced at the Goddard Space Flight Center with the software developed by the STIS Investigation Definition Team (IDT). Individual exposures were extracted following standard procedures for flatfielding and flux and wavelength calibration. Scattered light was removed using the scattered light correction developed by the STIS IDT, which accounts for echelle scatter as well as other sources of scattered light. Then the individual exposures were coadded weighted by their inverse variances averaged over a large region of one of the central orders. Finally, overlapping regions of adjacent orders were coadded again weighted by the inverse variance in each pixel, but in this case the variance vector was smoothed with a 5-pixel boxcar before being used for determination of the weighting so that noise fluctuations do not lead to inappropriate over or under-weighting. We initially reduced the data from the four observation dates separately. Careful inspection of the resulting four individual spectra reveals no significant variability. Consequently, we elected to coadd all of the data to obtain a single, high signal-to-noise spectrum. The total exposure time of the final spectrum is 78,198 seconds.

The overall appearance of the final spectrum of 3C351 is shown in Figure 1 (nine-pixel smoothing is used for this display, and the 1σ flux uncertainty is given). The broad O VI and Ly α emission lines are readily apparent. In this paper, we are mainly interested in the strong associated O VI and Ly α absorption lines visible on the blue side of the emission lines, as well as the associated N V lines near 1700 Å. The spike at 1216 Å is the geocoronal Ly α emission line, and the broad trough at 1216 is the damped Ly α absorption line due to H I in the Milky Way ISM. Some of the absorption lines in this spectrum are due to the low-redshift Ly α forest; investigation of these lines is valuable for understanding the nature and properties of the intergalactic medium in the nearby universe (e.g., Davé & Tripp 2001).

3. SPECTRAL MEASUREMENTS

3.1. Continuum and Emission Features

We used the *IRAF* task `specfit` (ver8.6) (Kriss 1994) to fit the STIS far-UV spectrum. The continuum was modeled as a power law, and only a Galactic extinction correction of $A_B = 0.097$ (Schlegel et al. 1998) was applied by using the reddening curve of Cardelli et al. (1989) with $R_V = 3.1$. The power-law index obtained is $\alpha = 0.0 \pm 0.029$, where $F_\lambda \propto \lambda^{-\alpha}$. The

observed flux in the continuum at 1500 Å is $\sim 1.5 \times 10^{-14}$ erg s⁻¹ cm⁻² Å⁻¹. The doublet O VI $\lambda\lambda$ 1032,1038 emission features are each fitted with a double Gaussian profile: a broader (FWHM $\sim 21,000$ km s⁻¹) component with a redshift of 0.3796 and a narrower (FWHM ~ 2400 km s⁻¹) component at $z = 0.3698$. The main fraction of the recombination emission originates in clouds in the broad emission-line region (BELR) that are optically thick in the ionizing continuum. The doublet flux ratio is found to be about 1:1 for both the broader and narrower components of the broad lines, which is reasonable for the optically thick physical conditions of the BELR (Hutchings et al. 2001). The doublet N V $\lambda\lambda$ 1238,1242 is located at the red edge of the STIS spectrum and separate emission-line components were not required in our fitting model.

For the strong Ly α emission profile, two Gaussians are used to give a good fit, one broad (FWHM $\sim 15,000$ km s⁻¹) and one narrow (FWHM ~ 3600 km s⁻¹). We also searched for emission lines from other Lyman lines, but if any are present they are very broad and weak (Our formal result finds only a broad emission component of Ly γ). For a clear physical picture of dynamics of the broad and narrow components in the BELR, we adopt the same rest-frame velocities for Ly α as those detected in the O VI doublet during the fitting of emission-line profiles. The radial velocities for the broad and narrow emission-line components with respect to the systemic redshift, $z_{em} = 0.3721 \pm 0.0003$ (2σ), obtained by Marziani et al. (1996) from the analyses of *FOS* UV spectra and ground-based optical spectroscopy (Boroson & Green 1992), are 1639 and -450 km s⁻¹, respectively. The emission fluxes and observed central wavelengths are listed in Table 2.

3.2. Associated Absorption Components

The high resolution and good S/N of this far-UV spectrum makes it possible to resolve unambiguously intrinsic absorption components in the O VI, N V and Lyman lines. In order to show all the distinct components of associated absorption, we present the blue wings of the high-ionization doublets O VI and N V in Fig. 2(a), and a similar diagram for the Lyman series in Fig. 2(b), where the fluxes are plotted as a function of the rest-frame velocity. There are in total 15 components detected in the associated absorption features (alphabetically, A – O), among which component G, with a relative velocity of -1699 km s⁻¹ (i.e., $z = 0.3644$), is the most striking one of either the high-excitation doublets or the Lyman series. An unusually strong metal line absorption system with a very close redshift ($z = 0.3646$) to component G was detected by Bahcall et al. (1993) in the intermediate-resolution ($R \sim 1300$) FOS spectroscopy, and it contains contributions from many of the components we resolve at 7 km s⁻¹ resolution. The FOS spectrum covers a wider wavelength range from 1180 Å to 3270 Å, and this strong metal absorption system is also seen in the C IV doublet $\lambda\lambda$ 1548,1550 at 2112.8 and 2116.6 Å, respectively. The STIS spectrum has such good resolution that component G in Ly ϵ is unblended with the Ly γ absorption from the intervening system at $z = 0.3175$, and even the

weak narrow associated absorption components, such as components K, M, N, and O, can be clearly resolved. We notice that components A (at $z = 0.3719$) and G appear in the Lyman series, O VI, and N V. The very narrow intrinsic components K, N and O are found only in O VI, and components B and J can be seen only in the Lyman series.

Additionally, the intergalactic metal-line absorption system at $z = 0.2210$ detected by Boissé et al. (1992) and Bahcall et al. (1993) is confirmed by the STIS spectrum. The line Si IV 1393Å of this intergalactic system appears in the domain (at 1701.8Å) of the N V doublet, and therefore is excluded in our measurement.

3.2.1. Associated Absorption Lines in the Doublets of O VI, N V and the Covering Factors

The intrinsic absorbers near the QSO might cover only part of the continuum or broad-line emitting sources along our line of sight (Hamann et al. 1997), and the covering factors could differ between ions and vary with velocity across the line profiles. The column density will be underestimated if this effect is not accounted for. In the case of single absorption lines (e.g., one component of Ly α absorption), we can derive a lower limit to the covering factor, C_f , along the line of sight from the residual flux, I_0 , in the core of the normalized absorption line at a particular radial velocity by $C_f \geq 1 - I_0$. For component B, the complete absorption in Ly α shows its covering factor is nearly 100% (i.e., $I_0 \approx 0$) (see Fig. 4). In practice, the actual value of the covering factor for a component can be determined only from a doublet, assuming both absorption lines of the doublet are unblended with other lines (Crenshaw et al. 1999). For the doublets O VI and N V in the STIS far-UV spectrum, the expected ratio of the optical depths of the doublet is ~ 2.0 , and the covering factor C_f can be derived by

$$C_f = \begin{cases} \frac{I_1^2 - 2I_1 + 1}{I_2 - 2I_1 + 1} & \text{for } I_1 > I_2 \geq I_1^2, \\ 1 & \text{for } I_2 < I_1^2, \\ 1 - I_1 & \text{for } I_2 \geq I_1, \end{cases} \quad (1)$$

where I_1 and I_2 are the normalized intensities in the weaker (e.g., O VI $\lambda 1037.6$) and stronger (e.g., O VI $\lambda 1031.9$) line troughs, respectively. In most cases, the value of I_2 is between I_1^2 and I_1 . If I_2 is outside of this range, it should be due to measurement uncertainties. The corresponding line optical depths of this doublet, (τ_1, τ_2) , are

$$\tau_2 = 2\tau_1 = 2 \ln \left(\frac{C_f}{I_1 + C_f - 1} \right). \quad (2)$$

To determine the covering factor of each component, we choose the high-ionization doublet O VI to start our fitting because it is continuous and has a higher signal-to-noise ratio as compared with the N V doublet. The absorption lines are treated as Gaussian profiles in optical depth $\tau(v_r)$, and the ratio of optical depths for this doublet is fixed at 2:1, assuming that the O VI and N V absorption lines are fully resolved. Most of the broad and smooth components

appear to be well resolved in the STIS spectrum. However, there are also narrow components that could, in principle, contain unresolved absorption. Theoretically, only components with temperatures less than 17,000 K would be still unresolved at 7 km s⁻¹ resolution.

Component A of Ly β is blended with the broad absorption component H of O VI, and its width and location are well constrained by its corresponding absorption profiles in O VI and Ly α . Since the width of component G is constrained by the corresponding spectral profiles of Ly β and Ly γ , the broadest absorption troughs in the O VI and Ly α lines around component G cannot be fitted by a single component, so components F and H were introduced. The associated absorption features in O VI were carefully deblended with 13 components (namely, A,C – I,K – O), and the resolving process is unambiguous. Fig. 3 shows the best fit to the O VI emission and absorption features. A strong narrow absorption is found at 1421.5Å, just between components A and C, and the possibility of being associated with 3C 351 can be ruled out. If it were an O VI λ 1038 absorption line, a stronger line of O VI λ 1032 should appear at 1413.3Å (see Fig 2a). Absence of the corresponding doublet absorption indicates that this feature is probably Lyman α in the intergalactic medium at $z = 0.1693$. Additionally, two narrow absorption lines resulting from intervening Ly α clouds can be found in the O VI region at 1413.938 and 1420.226 Å.

The STIS far-UV spectrum of the N V doublet at ~ 1700 Å has poorer S/N, as it appears on the red edge of the effective wavelength range. As seen in Fig. 2, only the strong associated components can be detected. We adopt the same values of rest-frame velocity, width, and covering factor for each component in N V as in O VI because both of these two species probably co-exist in the same high-ionization material. We achieved a good (in the χ^2 -sense) fit of the N V absorption features.

For fully resolved lines that have Gaussian distributions of optical depth, the column densities N_{ion} (in cm⁻²) can be derived by integrating the line optical depths across the absorption profiles by

$$\begin{aligned} N_{ion} &= \frac{m_e c}{\pi e^2 \lambda_0 f} \int \tau(v_r) dv_r = \left(\frac{m_e c}{\pi e^2}\right) \left(\frac{\pi}{4 \ln 2}\right)^{1/2} \left(\frac{\tau_0 W}{\lambda_0 f}\right) \\ &= 4.0108 \times 10^{14} \times \left(\frac{\tau_0 W}{\lambda_0 f}\right) \text{ (cm}^{-2}\text{)}, \end{aligned} \quad (3)$$

where λ_0 and f are the transition wavelength (in Å) and oscillator strength, which are cataloged by Morton (1991), τ_0 and W are central optical depth and width (i.e., FWHM in km s⁻¹) of the absorption line (Savage & Sembach 1991; Arav et al. 2001). The function ‘ptauabs’ in the latest version of the `specfit` task is used to parameterize absorption with partial covering of the continuum and BEL sources.

Table 3 presents the measurements of the associated absorption lines in these two doublets. We give the column density, line width (FWHM), rest-frame velocity, and covering factor for each component. The broadest component, E, is found to have the smallest covering factor in the O VI and N V doublets, and its column densities are even larger than those of component G. We emphasize that the column density N_{ion} and central optical depth $\tau(v_r)$ depend heavily upon

the covering factor, as shown in equations (2) and (3). It is well known that spectral resolution is crucial for accurate measurement of the associated absorption components in the doublets. Previous studies which are based on low-resolution ($R \sim 1000$) spectroscopic observations may have severe biases in column density determinations, since the blended complex of components in doublets in lower resolution spectra cannot be expected to result in any useful information about the covering factors.

3.2.2. Associated Absorption Lines in the Lyman series

Absorption features of the associated systems can be found in the Lyman lines, including all the major components (i.e., $\text{FWHM} > 20 \text{ km s}^{-1}$) that appear in the high-ionization O VI doublets. For these components we adopt the same values of the rest-frame velocity and width as those derived from the O VI fitting. The covering factors of absorption components in principle can be variable between different lines of the Lyman series since the BELR may be uncovered and each transition could therefore cover a different fraction of the total continuum plus emission line flux. However, permitting this extra freedom in the fitting could compromise the consistency of the results and so we initially set all lines to have the same covering factor. Some strong absorption components are found to have cores that are much deeper than the continuum flux levels (e.g., components A and B in Ly α), indicating that the regions responsible for the associated absorption lines lie completely outside of the BELR.

We fit the higher order Lyman lines (Ly β , Ly γ , Ly δ and Ly ϵ) simultaneously with Ly α since each is determined by the same neutral hydrogen column density and known oscillator strengths. We notice that there are strong emission features in Lyman α and O VI, whereas there are no obvious emission features in the higher order Lyman lines. Keeping in mind that the BELR may influence the covering factors for the associated Ly α absorbers, we force Ly α to have the minimum covering factor smaller than or equal to those of the higher order Lyman lines. In practice, we initially set the same values of the covering factors for the Lyman lines as those derived from O VI fitting, then permit the covering factors to vary only for the components whose fitting significantly deviates from the observed absorption features after adjusting the parameters of column density.

Table 4 lists the results of fits for the Lyman series, giving the column density, width, rest-frame velocity and covering factors in Lyman lines through Ly ϵ for each kinematic component. Fig. 4 shows the best fit to Ly α emission and the associated absorption lines. For component A, the width (i.e., FWHM) is restricted to be 23 km s^{-1} by the narrower absorption profile in O VI $\lambda 1038$, and its column density from the Lyman lines is also constrained by the corresponding unsaturated absorption features in Ly δ and Ly ϵ . This modeling fails to produce a good fit for component A in Ly α , but does fit the higher order Lyman lines very well. This might indicate that there exists additional low column density or low-ionization gas with a larger velocity dispersion at the same velocity, resulting in excess absorption seen only in Ly α .

Generally speaking, to model the same strength of absorption feature, absorbing gas with a smaller covering factor is required to have a higher column density. The covering factor of component E is held to be 100% for the Lyman lines, since its H I column density is strictly constrained by the fact that its corresponding absorption feature cannot be found in the Ly β or Ly δ lines. There is a deep trough at component G in Ly γ , even deeper than the corresponding troughs in Ly α and Ly β , so it is unlikely to result from only the material responsible for component G in Ly α and Ly β . This is likely to be an intergalactic Lyman α line at $z = 0.0915$ messing up this trough, so we excluded component G in Ly γ from our fit.

In addition to the components found in the O VI and N V lines, components B and J are detected in the Lyman lines. Only weak lower limits on their covering factors can be estimated from the residual flux at the absorption centers, and we assume their covering factors are 100% in our fitting.

4. PHYSICAL CONDITIONS OF THE ABSORBERS

It is well known that the ionization structure of photoionized gas is largely dependent upon the strength and shape of the incident continuum over a complete wavelength range, from the millimeter to X-ray bands. 3C 351 is a radio-loud and soft X-ray weak quasar whose spectral energy distribution (SED) is significantly different from the standard AGN continuum. Fortunately, a great volume of observational data in a variety of wavebands has been obtained for this quasar, which allows a more realistic modeling of the photoionized gas. Following Mathur et al. (1994), we use the continuum data from Elvis et al. (1994). The presence of the ionized absorber leads to uncertainty in determining the intrinsic X-ray spectral index α (for a power-law $f_\nu \propto \nu^{-\alpha}$). The extrapolation of the IR continuum is strongly limited by 1.3 mm observations (Antonucci & Barvainis 1988), and the slope in the submillimeter region is $-5/2$, similar to that of radio-quiet quasars. A detailed comparison of the observed continuum with the so-called “standard” AGN continuum can be found in Mathur et al. (1994).

To investigate the physical conditions of the intrinsic absorbers with photoionization models, we used the latest version of Cloudy (C94) (Ferland et al. 1998) in a similar way to Brotherton et al. (2002). A hydrogen volume density of 10^9 cm^{-3} and solar chemical abundance are assumed in our modeling. Based on the observed column densities of H I, N V and O VI for a specified kinematic component, we try to determine the total hydrogen column (N_H) and the ionization parameter (U) which is defined as

$$U = \frac{Q}{4\pi r^2 n_H c}, \quad (4)$$

where Q is the total number of ionizing photons per second, and n_H is the total number density of hydrogen. This method can lead to a unique solution for the major components which

have measurements of column density ratios of both $N(\text{O VI})/N(\text{H I})$ and $N(\text{N V})/N(\text{H I})$, namely components A, C, D, E, F, G, H and I. For components L and M which have only $N(\text{O VI})/N(\text{H I})$ measurements, the lack of a detectable N V line provides an upper limit for the column density, $\log N(\text{N V}) < 14.0$, which restricts double-valued solutions to the lower ionization parameter.

Instead of directly creating a large grid of models, we used the OPTIMIZE command in our computation to search for the model with the best fit of observed columns in an efficient way. We tried to test the dependence upon the hydrogen volume density n_H , and found that the modeling is not sensitive to the value of hydrogen density at all. Physical parameters for some absorption components are shown in Table 5. Note that most components have relatively low total column densities and ionization parameters.

4.1. Broad Absorption Features

The associated absorption features are dominated by the broad ($\text{FWHM} \geq 60 \text{ km s}^{-1}$) components with centroids shifted roughly from -781 to -2206 km s^{-1} . These components are marked above the spectrum in Fig. 3, including C, D, E, F, G and I. It is clear that all these broad components are found to have partial covering of the O VI line emission, which largely favors an intrinsic origin for the associated absorption systems. Note that most components are found to have ionization parameters of $0.13 < U < 0.32$, and total hydrogen columns of order 10^{19} cm^{-2} . Compared with the *ROSAT* PSPC values for the X-ray warm absorbers, $N_H \sim 1.4 \times 10^{22} \text{ cm}^{-2}$ and $U \sim 6.7$ (Mathur et al. 1994), the UV absorbing gas with physical conditions inferred from the STIS spectrum seems *not* to represent the same gas that is seen as the X-ray warm absorber.

In the STIS spectrum, component E has the widest velocity coverage (i.e., $\text{FWHM} \sim 381 \text{ km s}^{-1}$) and largest column densities for the O VI and N V doublets. It is also found to have the largest column density ratio of $N(\text{O VI})/N(\text{H I})$, which yields the highest ionization parameter of 0.32 and total hydrogen column of $1.55 \times 10^{19} \text{ cm}^{-2}$. Similarly, component D has a higher column density ratio of $N(\text{OVI})/N(\text{HI})$, and the resulting ionization parameter is also relatively high. Component G, with a width of 99 km s^{-1} and a rest-frame velocity of -1699 km s^{-1} , is found to have the largest column density for Lyman lines. This component has a comparatively smaller ratio of $N(\text{N V})/N(\text{H I})$ and a higher total hydrogen column density. Note that its covering factors are different for the high-ionization doublets ($\sim 80\%$), $\text{Ly}\alpha$ ($\sim 65\%$), and higher order Lyman lines ($\sim 100\%$).

Component C is measured to have the largest column density ratio of $N(\text{N V})/N(\text{H I})$, with a covering factor of $\sim 67\%$, but its physical condition is similar to components F, H, and I, with lower ionization parameter and total hydrogen column density. In addition, component L seems to be absent in N V $\lambda\lambda 1238, 1242$, and its column density ratio of $N(\text{O VI})/N(\text{H I})$ is

smaller. The corresponding absorber is modeled to have a lower ionization parameter of 0.095, under the constraint of $N(\text{N V}) < 10^{14} \text{ cm}^{-2}$.

4.2. Narrow Absorption Features

Component A appears in the Lyman lines and both high-ionization doublets, with the smallest outflow velocity, $\sim -37 \text{ km s}^{-1}$. The complete absorption at the line cores in $\text{Ly}\alpha$ and $\text{O VI } \lambda\lambda 1032, 1038$ might indicate that the absorber is located completely outside of the continuum and BELR of 3C 351. The ISM of the host galaxy is likely to be responsible for this narrow absorption component. However, the resulting lowest ionization parameter of 0.069 and its small rest-frame velocity might suggest that it is associated with the low-ionization gas in a putative rotating disk near the center of 3C 351. The absorption features in the Lyman lines at this component velocity cannot be well fitted by a single component with the same width of $\sim 23 \text{ km s}^{-1}$ as that of the O VI lines (see Fig. 4). The accretion disk might be the host of the inferred additional low-ionization absorbing gas.

Components K and M are clearly shown in the O VI doublet, and their covering factors for the O VI lines are determined to be 45% and 81%, respectively. The covering factor of component M for the Lyman lines is changed to 47%, and a lower ionization parameter is obtained with the constraint of $N(\text{N V}) < 10^{14} \text{ cm}^{-2}$. Component K is strongly blended with components M and L in $\text{Ly}\alpha$ and $\text{Ly}\beta$, and it is possible that some of the H I absorption that should have been assigned to component K was inadvertently assigned to components L or M instead. Additionally, components N and O may be present in $\text{Ly}\alpha$ line, but they fall in the low sensitivity or gaps between orders. We exclude these three components in our measurement. Taking the components B and J seen only in the Lyman lines into account, there are five components (plus K, N and O) with unknown relative ratios of $N(\text{O VI})/N(\text{H I})$ and $N(\text{N V})/N(\text{H I})$.

5. DISCUSSION

Based on the *HST* STIS spectrum of 3C 351, we derived the column density, covering factor, total hydrogen column and ionization parameter for each kinematic component. These quantities can help us determine if the gas responsible for the UV absorption features can also account for the X-ray absorption. As one of the very few X-ray-quiet quasars with an X-ray flux sufficient to obtain a spectrum with *ROSAT*, 3C 351 has been observed twice with the PSPC (Nicastro et al. 1999), and an ionized absorber is present, whose dominant feature is a strong O VII/O VIII absorption edge. The best fit to the PSPC spectrum taken on 1991 October, taking the preferred folded model with a break at 0.37 keV, leads to an ionization parameter $\log U$ of 0.78 – 1.08 and a total column density N_H of $1 - 2 \times 10^{22} \text{ cm}^{-2}$ (Mathur et

al. 1994). This ionization parameter U differs by a factor of ~ 30 from that inferred from the STIS far-UV spectrum, and the difference in total column density is much larger. The multiple kinematic components, low ionization parameters and total hydrogen column densities for most of the UV absorption indicate that the UV and X-ray absorption is unlikely to arise in the same material. Of course, there would be a possibility that the X-ray absorber was much weaker when the STIS observations were obtained, since the X-ray and STIS observations were taken years apart.

For the narrow absorption components B, J, K, N and O, for which the available absorption species are limited, we still can model the physical conditions, albeit with lower reliability. Component B is found to have only the low ionization solution: $\log U \sim -1.24$ and $\log N_H \sim 18.11$. However, two solutions, one with lower U and N_H , and another with higher U and N_H , are found with acceptable χ^2 values for components J, K, N and O. For these four components, we put the additional limit of $\log N(\text{C III}) < 12.5$ in the modeling, considering the non-detection of the C III λ 977 line, and two-fold solutions are still obtained. Therefore, it is possible that a unified UV-X-ray absorber still hides in these components. Components J and K are found to have similar higher ionization solutions of $\log U \sim 1.25$ and $\log N_H \sim 20.66$, as well as the lower ionization solutions: $\log U \sim -1.00$ and $\log N_H \sim 18.00$ for component J; $\log U \sim 0.03$ and $\log N_H \sim 18.02$ for component K. Components N and O seem to have similar high ionization solutions: $\log U \sim 1.29$ and $\log N_H \sim 20.72$, and their low ionization solutions show the low ionization parameters, $\log U \sim -1.20$ for component N and $\log U \sim -1.17$ for component O. The physical conditions for these four absorbers *may* be compatible with the X-ray warm absorber at this epoch, so the possibility that some UV and X-ray absorption arises in the same gas cannot yet be completely ruled out. Nevertheless our study suggests that the absorbers associated with quasars are complex outflows and that the UV and X-ray absorbing material are not identical for most individual kinematic components. This picture is consistent with the model proposed by Krolik & Kriss (2001), for which material with a wide range of physical conditions is stable.

As mentioned in §1, the radio properties of 3C 351 indicate an edge-on orientation of the accretion disk, which seems to be consistent with the unified geometry of the NAL and BAL absorbers detailed by Elvis (2000). According to this geometry, we look across the flow direction in NALs, while we look down the length of the flow in BALs (see Fig. 3 in Elvis 2000). The highest rest-frame velocity of the outflowing ionized gas along the line of sight reaches ~ 2800 km s $^{-1}$, so the absorbing gas outflowing approximately perpendicular to the accretion disk can be expected to have a much higher ejection velocity as shown in BALs ($0.1c - 0.2c$; Weymann et al. 1991).

There are techniques to derive additional information about the physical characteristics of the UV absorber. The density and distance to the central source of the associated absorber can be directly derived from time variability of absorption lines (Hamann et al. 1995), but this technique can not be applied for 3C 351 because it is a mildly variable quasar in the optical band, with a factor of ~ 2 variability on time scales of 5 – 10 yr (Grandi & Tifft 1974). In the

X-ray band, a factor of 1.7 change in flux within the nearly 2 years between repeated *ROSAT* PSPC observations is detected (Mathur et al. 1994). The four runs of STIS observations for 3C 351 failed to reveal significant UV variability over their time-frame, but some exploration is still possible. From the definitions of column density and ionization parameter U of the absorber (Eq. 4), the thickness and the distance to the central engine can be estimated from the gas density n_H . If some absorbers lie outside of the BELR, the constraints on the gas density can be used. As a result, we find that the UV absorbers may be close to the central engine of ~ 1 pc and a typical thickness of $\sim 10^{12}$ cm.

It is interesting to point out that all the broad absorption components (FWHM > 60 km s $^{-1}$) appeared in both the O VI and N V lines (i.e., components C, D, E, F, G, H and I) and have higher ionization parameters, ranging from 0.13 to 0.25, than those of the narrow components. This might indicate that the absorbing gas responsible for these broad absorption components is closer to the central emission source. The turbulence in rest-frame velocity might be an indicator of the location of the absorbing gas. However, we can't find a similar tendency in the UV spectra of other AGNs.

Strong associated metal line absorption has been observed in AGNs with soft X-ray absorption (Brandt, Laor, & Wills 2000). However, the disparity between the UV and X-ray absorbing gas has been illustrated clearly in a handful of Seyfert galaxies with both UV and X-ray observations. Only a small fraction have the UV absorber identified with the X-ray absorber. For example, one of seven components of intrinsic absorption in Seyfert 1 galaxy Mrk 509 is likely to be associated with the warm X-ray-absorbing gas, and the associated X-ray absorption for the other six components is negligible (Kriss et al. 2000). The high-resolution X-ray spectrum for another well-studied Seyfert 1 galaxy, NGC 5548, taken with the Low Energy Transmission Grating (LETG) on *Chandra*, shows strong narrow absorption lines with a blueshift of $\sim 280 \pm 70$ km s $^{-1}$, which may be identified with the UV absorbing gas responsible for either component 3 (Mathur et al. 1999) or 4 (Brotherton et al. 2002). However, high-resolution X-ray spectroscopy using *Chandra* has not yet been published for 3C 351, so the kinematic link of the UV components with the X-ray absorbers is not yet established.

We note the intriguing agreement in velocity among pairs of components in the O VI doublet. The short-wavelength member of component A is nearly centered in the long wavelength member of broad component G. Similarly, the $\lambda 1038$ lines of components N and O are superposed on the broad $\lambda 1032$ feature of component D. Line-locking is a possible cause of these velocity alignments (Srianand 2000), although chance superpositions in such a complex configuration must also be probable.

Though multiple kinematic components have been resolved in this STIS spectrum, the physical conditions of the absorbing gas are still poorly determined from absorption lines studies in the UV band alone. To unambiguously identify the UV absorption components with the X-ray warm absorbers, simultaneous high-resolution spectroscopic observations are still needed for 3C 351. The lack of X-ray spectroscopy of 3C 351 is currently a limit to better understanding

the relation between the warm absorbers and the UV associated absorbing gas.

6. SUMMARY

The *HST* STIS spectroscopy of 3C 351 provides a good chance to investigate the kinematic structure and physical conditions of the associated absorbers. The high-resolution far-UV spectrum of the radio-loud and X-ray-weak quasar 3C 351 shows strong emission lines from the O VI $\lambda\lambda$ 1032,1038 and Ly α lines, each of which can be resolved into two Gaussian profiles, one broad and one narrow. Kinematically complex associated absorption in 3C 351 is present on the blue wings of the high-ionization emission doublets O VI $\lambda\lambda$ 1032,1038, N V $\lambda\lambda$ 1238,1242 and Lyman lines through Ly ϵ . These absorption lines are resolved into several distinct kinematic components, spanning a rest-frame velocity range from -37 to -2800 km s $^{-1}$. All the broad absorption components are found to have partial covering of the background continuum source and the BELR, which strongly supports the intrinsic absorption origin and rules out the suggestion that the absorption arises in some associated cluster of galaxies. The column density ratios of N(O VI)/N(H I) and N(N V)/N(H I) are used to derive the physical conditions for some major associated absorbers, based on photoionization models. We find that all far-UV associated absorption components have low values of the ionization parameter and effective hydrogen column density, of which the higher ionization parameters are found for the absorbers responsible for the broad (FWHM > 60 km s $^{-1}$) absorption components. Although the low spectral resolution in the X-ray band in previous studies prevents a detailed comparison of the high-ionization resonance lines in the far-UV and X-ray spectra, we still can conclude that the UV and X-ray absorption are unlikely to arise in the same material, based on the multiple kinematic components, low ionization parameters and total hydrogen column densities we inferred for most of the UV absorbers.

The *STIS* observations were obtained for the STIS Instrument Definition Team. QY, RFG, TMT, and MEK acknowledge NASA support for IDT analysis. Additional support has been provided by NASA contract NAS5-30110. QY wants to acknowledge the financial support provided by the China Scholarship Council during the NOAO visit, the National Key Base Sciences Research Foundation under contract G1999075402, and the Chinese NSF No.19833008, 19873018.

REFERENCES

- Antonucci, R. R. J., & Barvainis, R. 1988, *ApJ*, 325, L21
- Arav, N., Brotherton, M. S., Becker, R. H., Gregg, M. D., White, R. L., Price, T., & Hack, W. 2001, *ApJ*, 545, 140
- Bahcall, J. N., et al. 1993, *ApJS*, 87, 1
- Becker R.H., et al. 2001, *ApJS*, 135, 227
- Boissé, P., Boulade, O., Kunth, D., Tytler, D., & Vigroux, L. 1992, *A&A*, 262, 401
- Boroson, T. A., & Green, R. F. 1992, *ApJS*, 80, 109
- Brandt, W. N., Laor, A., & Wills, B. J. 2000, *ApJ*, 528, 637
- Brotherton, M. S. 1996, *ApJS*, 102, 1
- Brotherton, M. S., Green, R. F., Kriss, G. A., Oegerle, W., Kaiser, M. E., Zheng, W., & Hutchings, J. 2002, *ApJ*(in press)
- Cardelli, J., Clayton, G. C., & Mathis, J. S. 1989, *ApJ*, 345, 245
- Crenshaw, D. M., Kraemer, S. B., Bogges, A., Maran, S. P., Mushotzky, R. F., & Wu, C. C. 1999, *ApJ*, 516, 750
- Davé, R., & Tripp, T. M. 2001, *ApJ*, 553, 528
- Ellingson, E., Yee, H. K. C., Bechtold, J., & Dobrzycki, A. 1994, *AJ*, 107, 1219
- Elvis, M., et al. 1994, *ApJS*, 95, 1
- Elvis, M. 2000, *ApJ*, 545, 63
- Ferland, G. J., Korista, K. T., Verner, D. A., Ferguson, J. W., Kingdon, J. B., & Verner, E. M. 1998, *PASP*, 110, 761
- Fiore, F., Elvis, M., Mathur, S., Wilkes, B., & McDowell, J. 1993, *ApJ*, 415, 129
- Foltz, C. B., Chaffee, F. H., Weymann, R. J., & Anderson, S. F. 1988, *Proceedings of the QSO Absorption Line Meeting*, ed. J.C. Blades, D. Turnshek, and C.A. Norman (Cambridge University Press), 53
- Gallagher, S. C., Brandt, W. N., Chartas, G., & Garmire, G. 2001, *ApJ*, (accepted) (astro-ph/0110579)
- George, I. M., Turner, T. J., Netzer, H., Nandra, K., Mushotzky, R. F., & Yaqoob, T. 1998, *ApJS*, 114, 73

- Grandi, S., & Tifft, W. G. 1974, *PASP*, 86, 873
- Green, P. J., Aldcroft, T. L., Mathur, S., Wilkes, B. J., & Elvis M. 2001, *ApJ*, 558, 109
- Hamann, F., Barlow, T.A., Beaver, E. A., Burbidge, E. M., Cohen, R. D., Junkkarinen, V., & Lyons, R. 1995, *ApJ*, 443, 606
- Hamann, F., Barlow, T. A., Junkkarinen, V., & Burbidge, E. M. 1997, *ApJ*, 478, 80
- Hutchings, J. B., Kriss, G. A., Green, R. F., Brotherton, M., Kaiser, M. E., Koratkar, A. P., & Zheng, W. 2001, *ApJ*, 559, 173
- Kellermann, K. I., Sramek, R., Schmidt, M., Shaffer, D. B., & Green, R. 1989, *AJ*, 98, 1195
- Kimble, R. A., et al. 1998, *ApJ*, 492, L83
- Kriss, G. A. 1994, *ASP Conf. Ser. 61: Astronomical Data Analysis Software and Systems III*, ed. D.R. Crabtree, R. J. Hanisch, and J. Barnes (San Francisco: Astronomical Society of the Pacific), 437
- Kriss, G. A., R. F. Green, M. Brotherton, et al. 2000, *ApJ*, 538, L17
- Krolik, J., & Kriss, G. A. 2001, *ApJ*, 561, 684
- Lanzetta, K. M., Bowen, D. V., Tytler, D., & Webb, J. K. 1995, *ApJ*, 442, 538
- Le Brun, V., Bergeron, J., & Boisse, P. 1996, *A&A*, 306, 691
- Marziani, P., Sulentic, J. W., Dultzin-Hacyan, D., Calvani, M., & Moles, M. 1996, *ApJS*, 104, 37
- Mathur, S., Wilkes, B., Elvis, M., and Fiore, F. 1994, *ApJ*, 434, 493
- Mathur, S., Elvis, M., Wilkes, B., 1999, *ApJ*, 519, 605
- Morton, D. C. 1991, *ApJS*, 77, 119
- Nicastro, F., Fiore, F., Perola, G. C., & Elvis, M. 1999, *ApJ*, 512, 136
- Reynolds, C. S. 1997, *MNRAS*, 286, 513
- Savage, B. D., & Sembach, K. R. 1991, *ApJ*, 379, 245
- Schlegel, D. J., Finkbeiner, D. P., & Davis, M. 1998, *ApJ*, 500, 525
- Srianand, R. 2000, *ApJ*, 528, 617
- Tananbaum, H., Avni, Y., Green, R. F., Schmidt, M., & Zamorani, G. 1986, *ApJ*, 305, 57

Weymann, R. J., Morris, S. L., Foltz, C. B., & Hewett, P. C. 1991, *ApJ*, 373, 23

Wilkes, B. J., Tananbaum, H., Worall, D. M., Avani, Y., Oey, M. S., & Flanagan, J. 1994,
ApJS, 92, 53

Woodgate, B. E., et al. 1998, *PASP*, 110, 1183

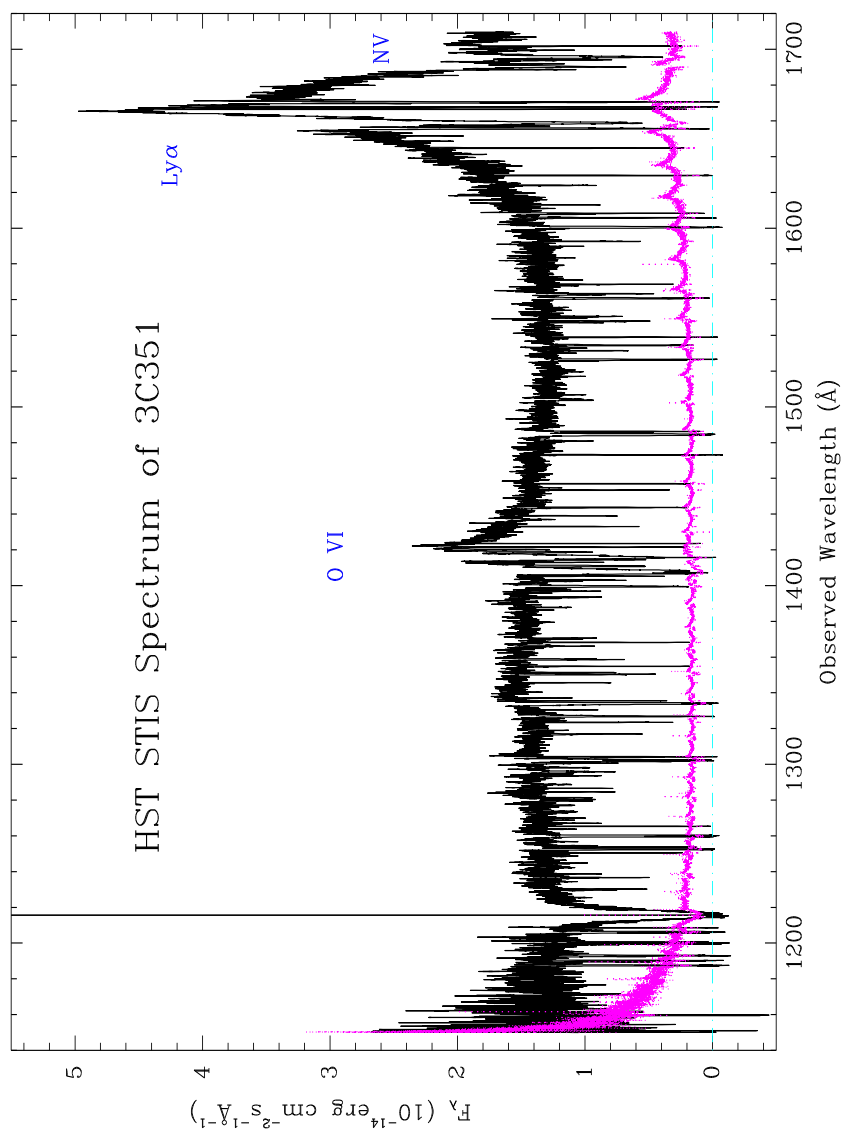


Fig. 1.— *HST* STIS far-UV spectrum of 3C 351, smoothed by 9 pixels. 1σ errors are shown as dotted lines. The spike at 1216 \AA is the geocoronal Ly α emission line, and the broad trough at 1216 \AA is the damped Ly α absorption line due to H I in the Milky Way ISM.

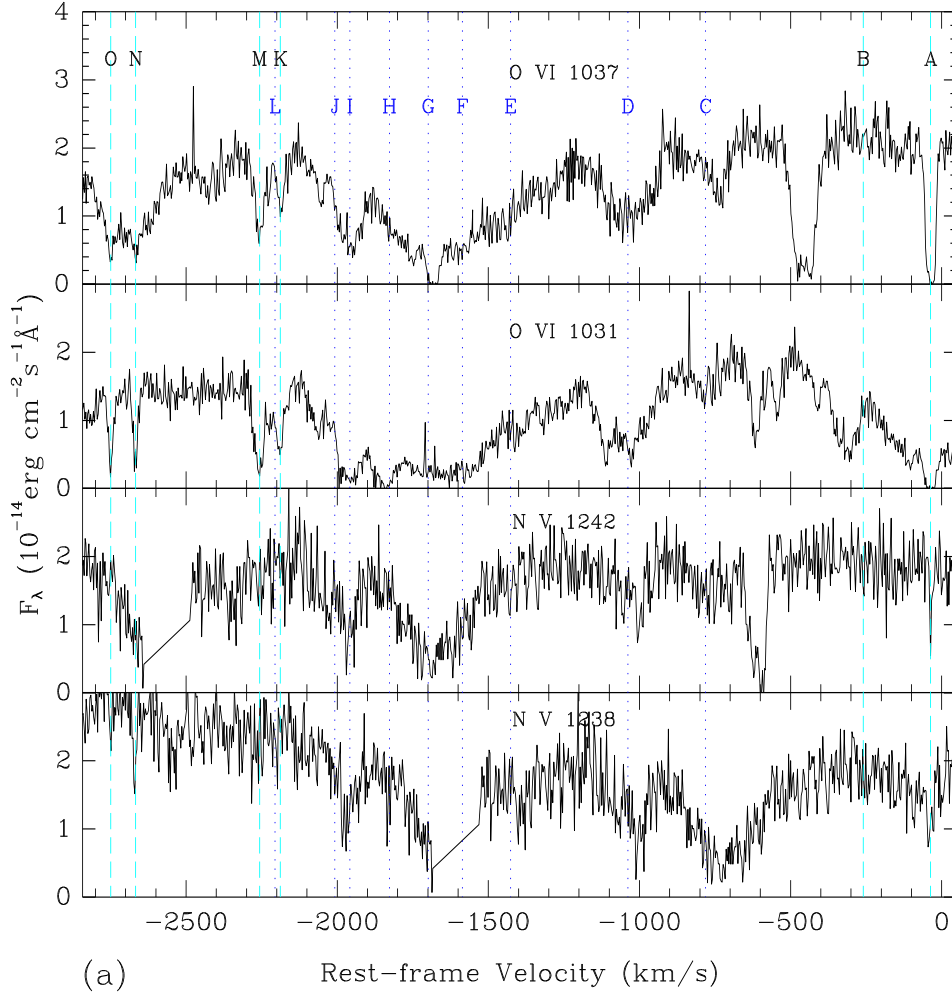
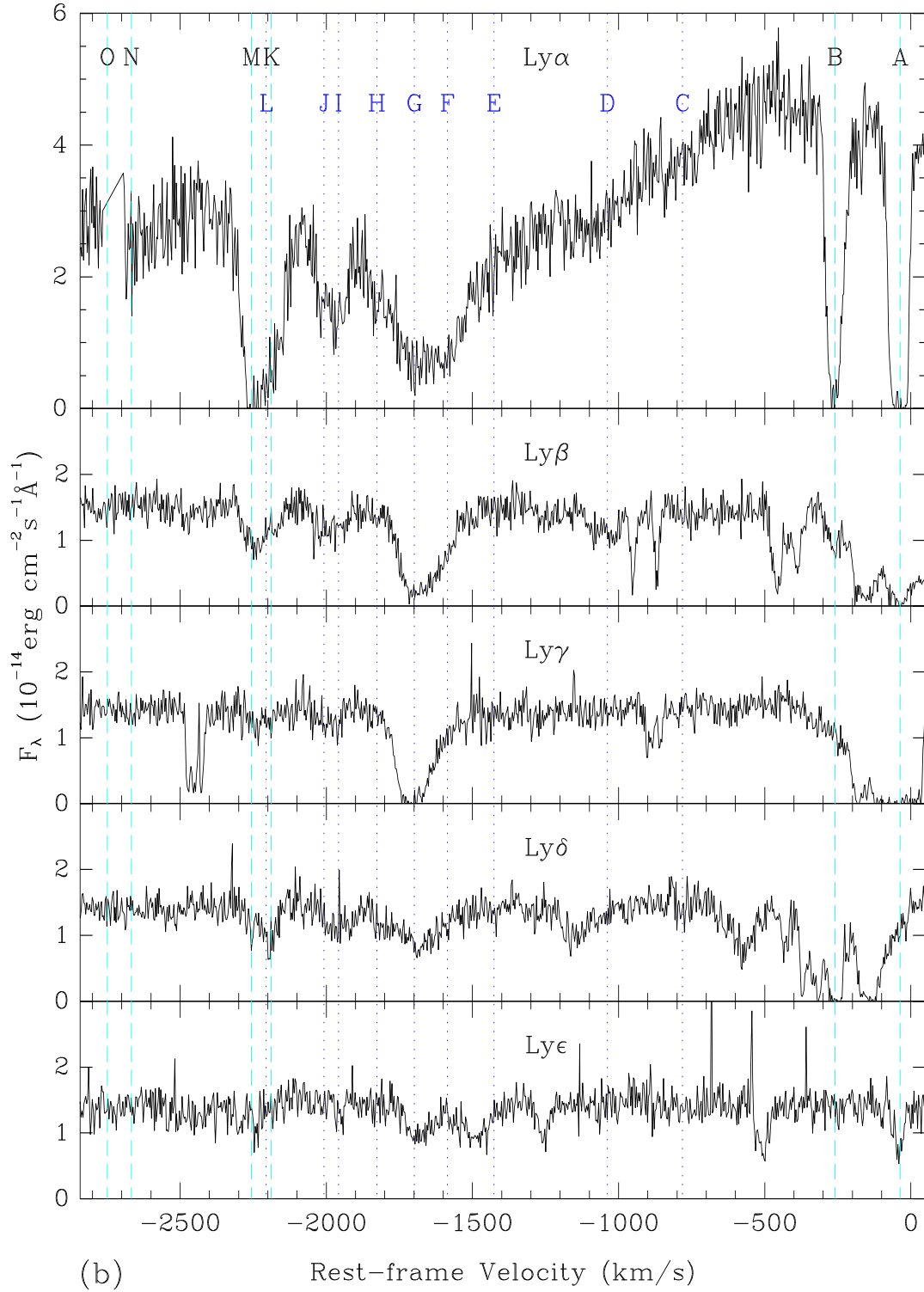


Fig. 2.— The associated absorption features in the rest-frame velocity domain. Fig. 2(a) is for the high-ionization doublets O VI and N V, and Fig. 2(b) for the Lyman series. The vertical dotted lines represent the broad absorption components ($\text{FWHM} > 60 \text{ km s}^{-1}$) and the dashed lines stand for narrow components ($\text{FWHM} < 60 \text{ km s}^{-1}$). The rest-frame velocity is relative to the systemic redshift of $z = 0.3721$. The covering factors for all these components can be well determined.



(b) Rest-frame Velocity (km/s)

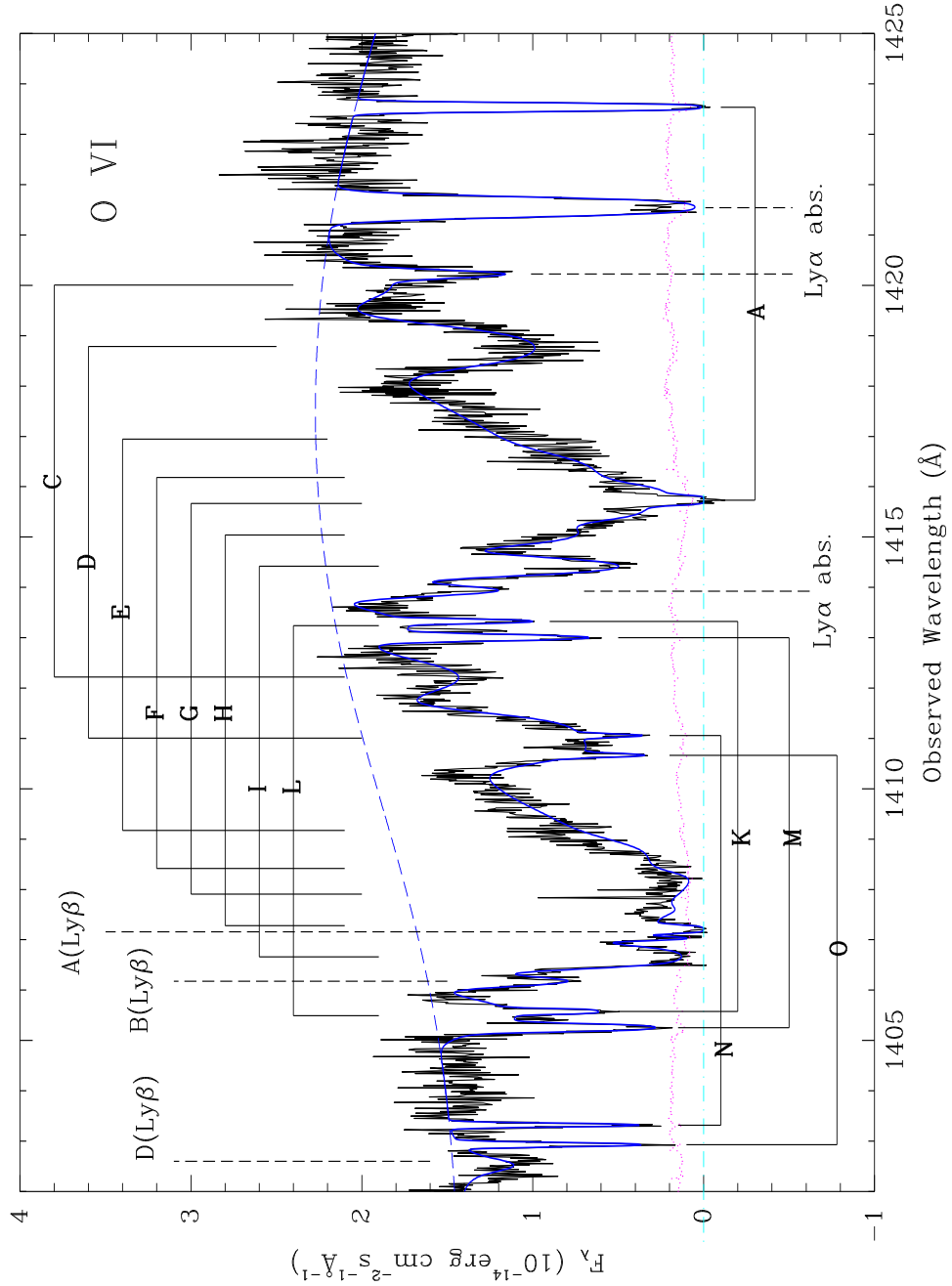


Fig. 3.— Spectrum of emission of the O VI doublet ($\lambda\lambda 1032, 1038$) (dashed line) with the best fit (solid line) to the associated absorption lines. The data are not binned, and 1σ errors are shown with dotted lines. The broad absorption components (FWHM $> 60 \text{ km s}^{-1}$) are marked with their designations above the spectrum, and the narrow components (FWHM $< 60 \text{ km s}^{-1}$) are marked below the spectrum. Some strong absorption features which do not belong to O VI are shown with dashed lines.

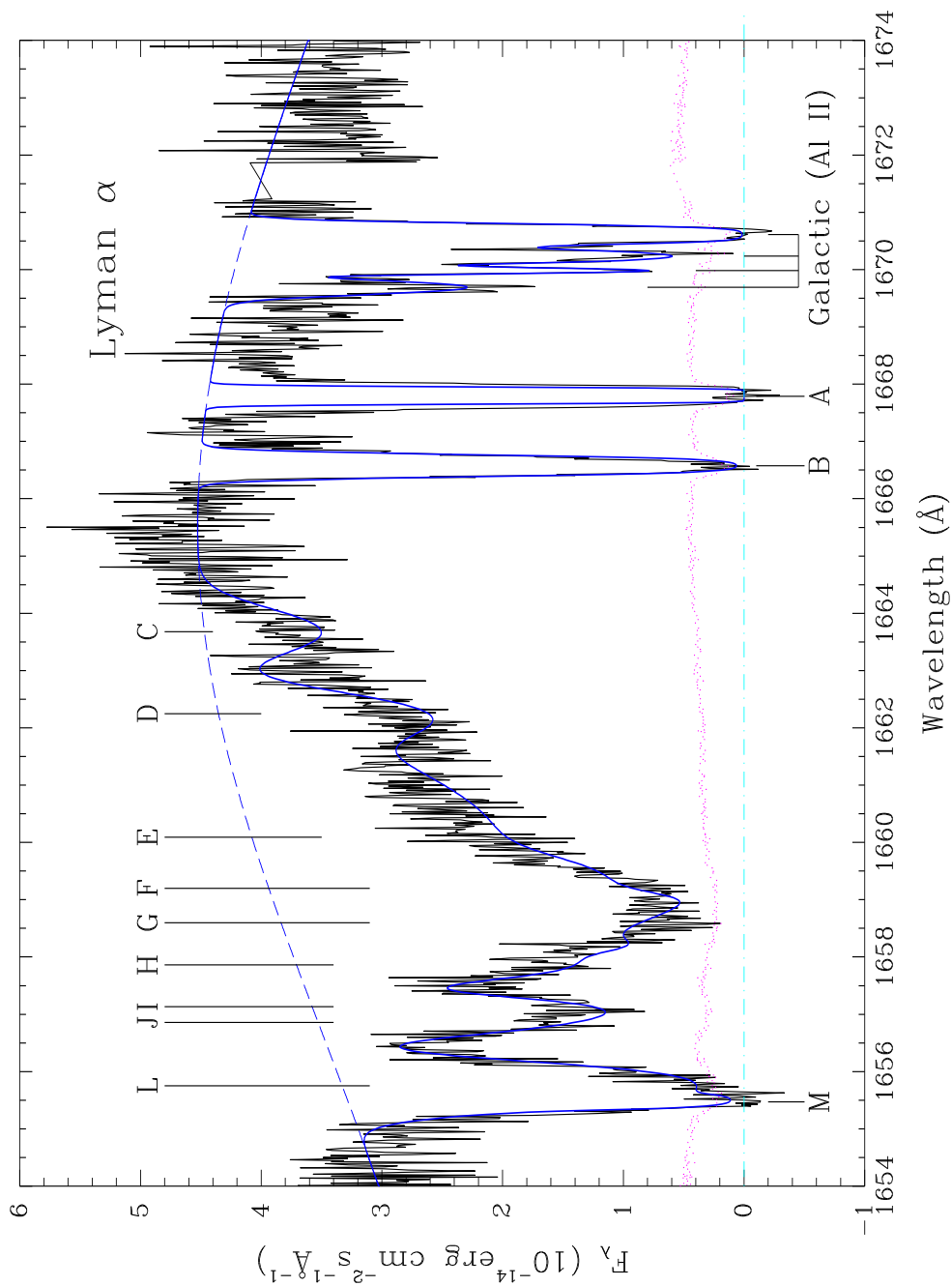


Fig. 4.— Spectrum of Ly α emission (dashed line) with the best fit (solid line) to the associated absorption lines. The data are not binned, and 1σ errors are shown with dotted lines. The broad absorption components (FWHM $> 60 \text{ km s}^{-1}$) are marked with their designations above the spectrum, and the narrow components (FWHM $< 60 \text{ km s}^{-1}$) are marked below the spectrum.

Table 1. Log of STIS Echelle Observations of 3C351

Observation Date	Total Integration Time (seconds)	<i>HST</i> Archive ID Codes
1999 June 27	19770	O57901010–O57901080
1999 June 29	14430	O57903010–O57903060
2000 Feb. 10	19770	O57902010–O57902080
2000 July 25	24228	O57904010–O579040A0

Table 2. Emission lines in *HST* STIS far-UV spectrum of 3C 351

Emission Lines	Observed λ ^a (Å)	Flux ^b (10^{-14} erg s ⁻¹ cm ⁻²)	FWHM ^a (km s ⁻¹)	Velocity (km s ⁻¹)
Broad O VI λ 1032	1423.64	11.0 ± 1.2	21041 ± 110	1639
Broad O VI λ 1038	1431.49	11.0 ± 1.7	21041	1639
Broad Ly α λ 1216	1677.14 ± 0.02	85.5 ± 4.0	15001 ± 684	1639 ± 4
Broad Ly γ λ 973	1341.70	15.0 ± 1.4	21041	1639
Narrow O VI λ 1032	1413.56 ± 0.15	6.8 ± 0.5	2402 ± 31	-450 ± 32
Narrow O VI λ 1038	1421.36	6.8 ± 0.3	2402	-450
Narrow Ly α λ 1216	1665.26	49.8 ± 2.2	3601 ± 329	-450

^aValues without uncertainties are either tied to another parameter or become fixed during the profile fitting.

^bCorrected for $E_{B-V} = 0.023$, $R_V = 3.1$ (Cardelli et al. 1989).

Table 3. Associated absorption lines of O VI and N V doublets

Feature	Column density ^a (10^{12} cm^{-2})	FWHM ^b (km s^{-1})	Velocity ^{b,c} (km s^{-1})	Covering ^b Fraction
O VI $\lambda\lambda 1032, 1038$				
A	490 ± 66	23 ± 1	-37 ± 4	1.00
C	214 ± 16	155 ± 24	-781 ± 16	0.67 ± 0.05
D	1238 ± 107	138 ± 8	-1038 ± 9	0.62 ± 0.02
E	3697 ± 271	381 ± 11	-1426 ± 26	0.39 ± 0.02
F	1186 ± 94	156 ± 13	-1586 ± 10	0.70 ± 0.01
G	2238 ± 59	99 ± 4	-1699 ± 5	0.80 ± 0.03
H	626 ± 80	101 ± 2	-1827 ± 6	0.85 ± 0.04
I	541 ± 38	75 ± 4	-1958 ± 5	0.96 ± 0.08
K	185 ± 75	14 ± 1	-2188 ± 5	0.45 ± 0.09
L	314 ± 53	116 ± 10	-2206 ± 11	0.42 ± 0.01
M	159 ± 148	23 ± 6	-2257 ± 6	0.81 ± 0.08
N	46 ± 15	14 ± 10	-2667 ± 5	0.98 ± 0.13
O	69 ± 20	16 ± 2	-2749 ± 5	0.86 ± 0.21
N V $\lambda\lambda 1238, 1242$				
A	25 ± 5	23	-37	1.00
C	239 ± 67	155	-781	0.67
D	134 ± 42	138	-1038	0.62
E	708 ± 22	381	-1426	0.39
F	395 ± 42	156	-1586	0.70
G	367 ± 8	99	-1699	0.80
H	59 ± 23	101	-1827	0.85
I	81 ± 24	75	-1958	0.96

^aCorrected for $E_{B-V} = 0.023$, $R_V = 3.1$ (Cardelli et al. 1989).

^bValues without uncertainties are either tied to another parameter or become fixed during profile fitting.

^cVelocities are relative to the systemic $z_e = 0.3721 \pm 0.0003$ (2σ) (Marziani et al. 1996). The uncertainty includes the spectral resolution and fitting error.

Table 4. Associated absorption lines of Lyman series

Feature	Column density ^a (10^{12} cm^{-2})	FWHM (km s^{-1})	Velocity ^{b,c} (km s^{-1})	Covering factor ^b				
				Ly α	Ly β	Ly γ	Ly δ	Ly ϵ
A	446 ± 5	23	-37	1.00	1.00	1.00	1.00	1.00
B	106 ± 5	43 ± 3	-260 ± 4	1.00	1.00	1.00	1.00	–
C	35 ± 2	155	-781	0.67	–	–	–	–
D	55 ± 12	138	-1038	0.62	0.62	–	–	–
E	144 ± 19	381	-1426	1.00	–	–	–	–
F	147 ± 33	156	-1586	0.70	1.00	1.00	–	–
G	629 ± 211	99	-1699	0.65 ± 0.06	1.00	–	1.00	1.00
H	70 ± 7	101	-1827	0.85	0.85	0.85	0.85	–
I	35 ± 5	75	-1958	0.96	0.96	0.96	0.96	–
J	36 ± 6	90	-2008 ± 49	1.00	1.00	–	–	–
L	144 ± 32	116	-2206	1.00	1.00	–	–	–
M	124 ± 20	23	-2257	0.47 ± 0.31	0.47	–	–	–

^{a,b,c} Notes are given in Table 3

Table 5. Photoionization models for the major kinematic components

Components	Velocity (km s ⁻¹)	N(OVI)/N(HI)	N(NV)/N(HI)	log U	log N_H (cm ⁻²)
A	-37	1.10	0.06	-1.16	18.36
C	-781	6.11	6.83	-0.86	18.37
D	-1038	22.51	2.44	-0.51	18.65
E	-1426	25.67	4.92	-0.50	19.19
F	-1586	8.07	2.69	-0.76	18.86
G	-1699	3.56	0.58	-0.91	19.10
H	-1827	8.94	0.84	-0.71	18.39
I	-1958	15.46	2.31	-0.63	18.36
L	-2206	2.18	–	-1.02	18.43
M	-2257	1.28	–	-1.13	18.30